OPEN

Evaluating the Image Quality of Monoenergetic Images From Dual-Energy Computed Tomography With Low-Concentration and Low-Flow-Rate Contrast Media for the Arterials Supply to the Nipple-Areola Complex in Breast Cancer Compared With Conventional Computed Tomography Angiography

Xiangfei Zeng, BS, Xiaoxia Wang, MS, Huifang Chen, MS, Daihong Liu, MD, Jinfang Shi, BS, Jing Zhang, MS, Xiaoqin Li, BS, Liyin Zhang, BS, Yi Yang, BS, and Jiuquan Zhang, MD

Objective: The objective of this study was to evaluate the image quality of monoenergetic images (MEIs (+)) acquired from dual-energy computed tomography with low-concentration and low-flow-rate contrast media for the arterial supply to the nipple-areola complex (NAC) in breast cancer compared with conventional computed tomography angiography (CTA).

Methods: We enrolled 25 patients (MEI $(+)_{300}$ group, 300 mg/mL and 2.5 mL/s of contrast media) and 23 patients (CTA_{370} group, 370 mg/mL and 3.5 mL/s of contrast media) for assessing NAC blood supply angiography. The image quality of the 2 groups was evaluated objectively and subjectively.

Results: The 40 keV MEI $(+)_{300}$ demonstrated higher attenuation and contrast-to-noise ratio than CTA_{370} group ($P < 0.001$). The subjective image quality and visualization of the arteries were comparable between 2 groups.

Conclusions: The 40 keV MEI $(+)_{300}$ acquired from dual-energy computed tomography can achieve comparable image quality of arterial supply to NAC with low-concentration and low-flow-rate contrast media in breast cancer compared with CTA_{370}.

Key Words: dual-energy CT, CT angiography, monoenergetic image, nipple-areola complex

(*J Comput Assist Tomogr* 2020;44: 921–927)

From the Department of Radiology, Chongqing University Cancer Hospital & Chongqing Cancer Hospital, & Chongqing Cancer Institute, Chongqing, P. R. China.

Received for publication March 30, 2020; accepted May 27, 2020.

Correspondence to: Jiuquan Zhang, MD, Department of Radiology, Chongqing University Cancer Hospital, No. 181 Hanyu Rd, Shapingba District, Chongqing 400030, P. R. China (e-mail: zhangjq_radiol@foxmail.com).

This study has received funding by the Achievement Encourage's specific projects for Chongqing Research Institutes (grant number cstc2018jxjl130072), combined medicine and engineering projects of the Fundamental Research Funds for the Central Universities in 2019 (project number 2019CDYGYB008), the Chongqing Key Medical Research's combined science and medicine project (grant number 2019ZDXM007), and the 2019 SKY Imaging Research Fund of the Chinese International Medical Foundation (project number Z-2014-07-1912-10).

Xiangfei Zeng and Xiaoxia Wang are co-first authors and contributed equally to the study.

The authors declare no conflict of interest.

DOI: 10.1097/RCT.0000000000001063

Breast cancer is the most frequently diagnosed cancer among women and is the leading cause of cancer death in many countries.[1] As a result of early detection, improved adjuvant therapy, and a better understanding of tumor biology, more patients with breast cancer choose breast-conserving therapies. Nipple-sparing mastectomy (NSM) is a new surgical approach characterized by the preservation of the entire nipple-areola complex (NAC) and breast skin envelope during mastectomy, thereby promoting superior esthetic outcomes and improving quality of life when combined with immediate breast reconstruction.[2] However, one potential pitfall of NSM is the uncertainty of the arterial supply to the NAC, which is important to consider to ensure perfusion to the NAC before choosing the vascular pedicle.[3] Previous anatomical studies[3–5] have revealed that the arterial supply to the NAC originates from vascular sources such as the internal thoracic artery, lateral thoracic artery, thoracoacromial artery, intercostal artery, and axillary artery. However, many studies[5–7] have also shown that the arterial supply pattern of the NAC is highly variable across individuals. Therefore, it is an increasingly common practice in NSM to plan procedures using noninvasive imaging technologies to map the vascular anatomy preoperatively to confirm the location, size, and source of the arterial supply to the NAC.

Computed tomography angiography (CTA) is considered the criterion standard for preoperative vascular imaging in vivo[8,9] because it can display the complete outline of the breast vascular map preoperatively by 3-dimensional visualization in a manner that is robust, accurate, intuitive, and of satisfactory resolution. In addition, CTA has proven to be an excellent predictor of sensitivity and positivity, and several studies[10,11] have demonstrated that routine preoperative use of CTA can shorten surgery time and reduce emotional stress for the surgeon as well as the number of postoperative complications. With the advent of rapid CTA scanning patterns, administration of contrast media with a high iodine concentration (ie, 370–400 mg/mL) and high-flow-rate injection modes have become routine clinical practices to maximize arterial enhancement in the systemic circulation.[12–14] The concomitant disadvantage of CTA is that it can increase the risk of contrast media-induced acute kidney injury,[15,16] and the relatively large quantity of high viscosity contrast media could place an increased strain on the vein wall, increasing the risk of extravasation.[17]

Previous studies[16,18–20] have shown that low–kiloelectron volt monoenergetic images (MEIs (+)) from dual-energy computed tomography (DECT) constitute a useful protocol for CTA, demonstrating superior iodine contrast enhancement with a low dose of contrast media compared with that of conventional CTA. In a

study of chest CTA,[13] the authors found that the image quality of MEIs (+) at 60 keV with low-concentration contrast media (170 mg/mL) was comparable with that of single-energy computed tomography (CT) with high-concentration contrast media (350 mg/mL). To date, few comparative studies have compared the image quality between MEIs (+) obtained with low-concentration and flow-rate contrast media and conventional CTA images for the preoperative imaging of the arterial supply to the NAC.

We hypothesized that MEIs (+) acquired from DECT can improve the attenuation of the arterial supply to the NAC with low-concentration and low-flow-rate contrast media. In our study, DECT was performed for a MEI $(+)_{300}$ group (300 mg/mL, 2.5 mL/s of contrast media) and a CTA_{370} group (370 mg/mL, 3.5 mL/s of contrast media) with breast cancer, and the attenuation and SD of the 5 arterials supply to the NAC were measured in the MEI $(+)_{300}$ and CTA_{370} groups individually. The purpose of our study was to evaluate the imaging quality of MEIs (+) acquired from DECT with low-concentration and low-flow-rate contrast media for the arterial supply to the NAC in breast cancer compared with conventional CTA.

MATERIALS AND METHODS

Patient Characteristics

Our prospective, single-center study was approved by the ethics committee of our hospital, and written informed consent was obtained from all participants. A total of 48 patients with histopathologically proven primary breast tumors who had been admitted to our hospital between June 2019 and January 2020 were included. The MEI $(+)_{300}$ group (25 participants) underwent DECT of the thorax for the staging of lung metastasis. The CTA_{370} group (23 participants) underwent DECT of the thorax for preoperative NAC blood supply angiography. Inclusion criteria included a first diagnosis of breast cancer and a lack of history of chemotherapy or radiation therapy in the breast space. The exclusion criteria for DECT were based on the clinical guidelines for contrast-enhanced CT at our institution: impaired kidney function (glomerular filtration rate, <30 mL/min), history of severe contrast media allergy, pregnancy, and inability to give informed consent for the CT examination.

DECT Image Acquisition

Image data were acquired on a 2.5 generation dual-source CT unit (SOMATOM Drive; Siemens Healthineers, Forchheim, Germany) in dual-energy mode using a tin filter for the high-voltage tube. An automatic exposure control system (CARE Dose4D; Siemens Healthineers) was used for all scans. All patients were scanned craniocaudally in the supine position with the bilateral arms elevated in close contact with the head. The whole chest was scanned from the superior aperture of the thorax to the inferior edge of the costophrenic angle during a deep-inspiratory breath hold, covering the breast and axillary areas. For contrast-enhanced scanning, contrast media were administered through the right or left ulnar vein by a dual-head injector. The ulnar vein contralateral to the suspected breast lesion was selected to avoid beam hardening artifacts of the axillary vein. The scanning and injection protocols for the 2 groups are described in Table 1.

TABLE 1. Scanning and Injection Protocols in 2 Groups

Parameter	MEI $(+)_{300}$ Group (n = 25)	CTA_{370} Group (n = 23)
Scanning parameters		
Tube voltage, kVp	80 (Tube A)/Sn140 (tube B)	80 (Tube A)/Sn140 (tube B)
Blending factor	0.6	0.6
Reference tube current time product, mAs	71 (Tube A)/60 (tube B)	71 (Tube A)/60 (tube B)
Rotation time, s	0.28	0.28
Pitch	0.55	0.55
Collimation, mm	64 × 0.6	64 × 0.6
Reformatted section thickness, mm	1.5	1.5
Reformatted section increment, mm	1.5	1.5
ADMIRE level	2	2
Kernels (mediastinum)	Q30f	Q30f
Threshold of bolus-tracking (region of interest in ascending aorta), HU	100	120
Delay time, s	10	10
Injection parameters		
Contrast media	Iohexol (Yangzijiang, Jiangsu, China)	Iopromide (Bayer AG, Berlin, Germany)
Iodine concentration, mg/mL	300	370
Ion type	Nonionic	Nonionic
No. benzene rings	1	1
Viscosity (37°C), cP	6.1	10
Osmotic molecular concentration (37°C), osm/kg	0.64	0.77
Volume, mL/kg	1.2	1.5
Flow rate, mL/s	2.5	3.5
Iodine content, mg/kg	360	555
Injection mode	2 Phase, bolus injection	2 Phase, bolus injection
Physiological saline volume, mL	30	30
Physiological saline flow rate, mL/s	2.5	3.5

ADMIRE indicates Advanced Modeled Iterative Reconstruction.

DECT Image Reconstruction

Reconstructed CT image data were postprocessed on a syngo.via workstation (syngo.via VB20A, Dual Energy; Siemens Healthineers). In the MEI $(+)_{300}$ group, noise optimized MEIs (+) were reconstructed at 40, 50, 60, 70, and 80 keV. In the CTA_{370} group, standard linear-blended polyenergetic image were reconstructed by applying a blending factor of 0.6 (M_0.6; 60% of the low-kilovolt spectrum and 40% of the high-kilovolt spectrum). Multiplanar reformations were generated for the optimal MEI $(+)_{300}$ and CTA_{370} groups in the same workstation. Multiplanar reformations were reconstructed in the coronal plane with 20-mm section thickness and no intersection gap with the maximum intensity projection method. All image data sets, including reformatted images and axial images, were archived to a picture archiving and communication system for interpretation.

Objective Image Analysis

For quantitative evaluation, parameters were measured by 2 radiologists (X.W., with 7 years of experience in breast and chest diagnostic imaging, and X.Z., with 2 years of experience in

postreconstruction imaging). We measured the attenuation (Hounsfield units) and SD by placing a manually defined region of interest on all axial images for the 5 arterials supply of the NAC (internal thoracic artery, lateral thoracic artery, thoracoacromial artery, intercostal artery, and axillary artery) and the ipsilateral pectoral muscle with breast cancer. Regions of interest were drawn as large as the vessel lumen, and wall calcifications that might cause artifacts were avoided. The mean attenuation and SD were calculated for each patient by averaging the values from the 5 arterials supply of the NAC. The contrast-to-noise ratio (CNR) and signal-to-noise ratio (SNR) were calculated according to the following formulas:

$$\mathrm{CNR} = (\mathrm{Hu}_{vessel} - \mathrm{Hu}_{muscle})/\mathrm{SD}_{(\mathrm{air})}$$

$$\mathrm{SNR} = \mathrm{Hu}_{vessel}/\mathrm{SD}_{(\mathrm{air})}$$

Subjective Image Analysis

Subjective imaging data were performed by the same 2 radiologists who obtained the quantitative parameters. They were unaware of the DECT scanning parameters and reviewed the multiplanar reformations MEI $(+)_{300}$ image with the highest CNR and SNR among the MEIs $(+)_{300}$ and CTA_{370} groups at the same window width and window level after objective image analysis 1 month later independently. When evaluating the 2 groups of images, source blood vessels that either extended directly or had branches or perforators winding distally into the NAC regions were defined as the dominant vessels for NAC perfusion.[5] Then, each dominant vessel was identified and ascribed to a corresponding source vessel that included the internal thoracic artery, the lateral thoracic artery, the thoracoacromial artery, the intercostal artery, and other arteries likely to be the source vessels for NAC perfusion. The image quality was assessed with a subjective 5-point scale system[16] based on the overall clarity of the anatomic vascular details. Image quality was scored as follows: 5, sharp anatomical structure and satisfactory details; 4, less clear anatomical structure and details;

TABLE 2. Patient Demographics, Tumor Characteristics, and Radiation Dose of 48 Patients With Breast Cancer in MEI $(+)_{300}$ and CTA_{370} Groups

Characteristics	MEI $(+)_{300}$ Group (n = 25)	CTA_{370} Group (n = 23)	*P*
Age, y	50.92 ± 9.25	50.58 ± 10.06	0.90
Weight, kg	56.58 ± 4.73	56.33 ± 7.26	0.89
Height, cm	154.11 ± 6.20	154.98 ± 5.12	0.98
BMI, kg/m^2	23.90 ± 2.19	23.89 ± 3.80	0.98
Diabetes	2 (8.0%)	1 (4.3%)	1.00
Hypertension	3 (12.0%)	2 (8.7%)	1.00
Menstruation state			
Premenopausal women	13 (52.0%)	13 (56.5%)	0.75
Postmenopausal women	12 (48.0%)	10 (43.5%)	
The maximal tumor diameter, cm	3.06 ± 0.95	2.60 ± 1.57	0.23
Mass position			
Outer upper quadrant	14 (56.0%)	10 (43.5%)	0.85
Outer lower quadrant	5 (20.0%)	6 (26.1%)	
Inner upper quadrant	3 (12.0%)	3 (13.0%)	
Inner lower quadrant	3 (12.0%)	4 (17.4%)	
Concomitant signs			
Nipple depression/skin thickening	3 (12.0%)	0 (0%)	0.24
No. cases of positive lymph nodes	6 (24.0%)	1 (4.3%)	0.10
DLP	5.35 ± 1.10	5.02 ± 1.87	0.66
CTDI vol	160.6 ± 71.94	156.3 ± 74.7	0.17

Data are presented as mean ± SD.

BMI indicates body mass index; CTDI vol, CT dose index volume; DLP, dose length product.

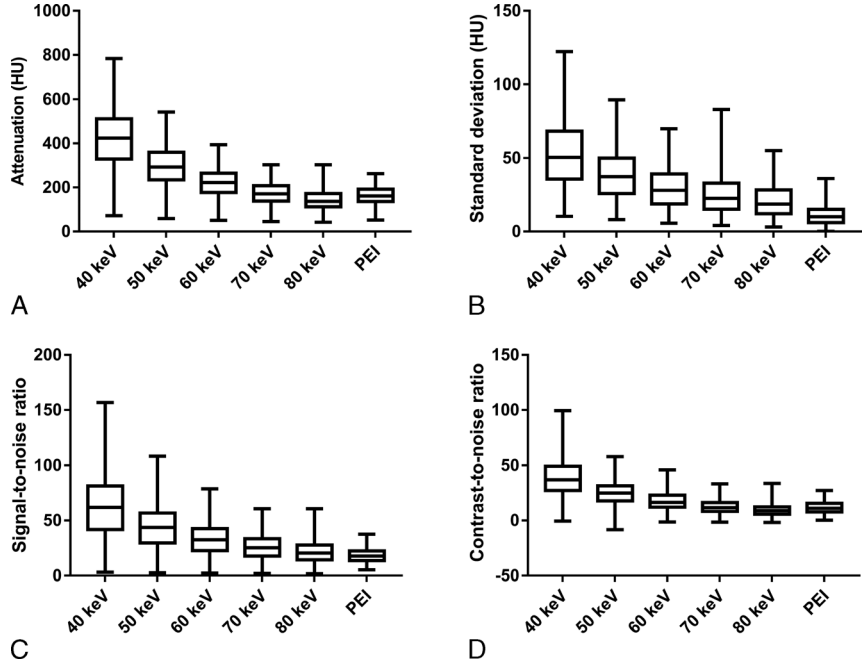

FIGURE 1. Quantitative indexes across the range of virtual monochromatic energy levels (40–80 keV) and PEI reconstructed from DECT in the MEI $(+)_{300}$ group: (A) attenuation, (B) SD, (C) SNR, and (D) CNR. Maximum attenuation, SD, SNR, and CNR occurred at 40 keV MEI $(+)_{300}$. PEI, standard linear-blended polyenergetic image (60% of the low-kilovolt spectrum and 40% of the high-kilovolt spectrum).

TABLE 3. Objective Analysis of Images Between the 40 keV MEI $(+)_{300}$ Group and CTA_{370} Group

Parameters	40 keV MEI $(+)_{300}$ Group	CTA_{370} Group	*P*
Attenuation			
Axillary artery	591.83 ± 87.71	256.74 ± 48.54	<0.001
Thoracoacromial artery	424.05 ± 103.69	216.09 ± 45.71	<0.001
Lateral thoracic artery	368.80 ± 89.53	214.74 ± 45.04	<0.001
Internal thoracic artery	348.02 ± 105.92	215.52 ± 45.85	<0.001
Intercostal artery	410.91 ± 74.16	221.91 ± 55.75	<0.001
Mean attenuation	428.72 ± 125.80	225.00 ± 50.15	<0.001
SD			
Axillary artery	44.70 ± 14.89	18.34 ± 8.9	<0.001
Thoracoacromial artery	50.05 ± 24.09	16.56 ± 12.75	<0.001
Lateral thoracic artery	63.82 ± 31.44	15.39 ± 8.00	<0.001
Internal thoracic artery	49.7 ± 18.54	18.82 ± 8.67	<0.001
Intercostal artery	58.44 ± 21.96	24.82 ± 15.87	<0.001
Mean noise	53.37 ± 23.54	18.79 ± 11.53	<0.001
SNR	64.78 ± 28.50	26.29 ± 8.68	<0.001
CNR	55.92 ± 27.15	18.79 ± 7.46	<0.001

Data are presented as mean ± SD.

3, decreased confidence in details but anatomical structure still relatively clear; 2, poor details and anatomical structure decreased; and 1, unacceptable anatomical structure and details. The visualization of the arterials supply to the NAC was assessed on a 3-point scale: 0, inadequate visualization; 1, adequate visualization; and 2, excellent visualization.

Statistical Analysis

Statistical analyses were performed using commercially available statistical software (SPSS software, version 25.0; Armonk, NY). Interobserver variability and statistical analyses were calculated for every pairwise combination of observers. A 2-way random intraclass correlation coefficient model with absolute agreement, single measures, and 95% confidence interval was used. Quantitative data (age, height, weight, body mass index, maximal tumor diameter, radiation dose, attenuation, SD, SNR, and CNR) are presented as the means ± SDs and were compared using the independent samples *t* test. The characteristics of the 2 groups (menstruation state, prevalence of diabetes and hypertension, tumor position, and concomitant signs) were assessed using the χ^2 or Fisher exact test. For qualitative analysis, the differences between the subjective scores of 2 groups were tested with the Mann-Whitney *U* test. The level of significance was defined as $P < 0.05$.

RESULTS

Patient Characteristics

The 2 groups' demographics, tumor characteristics, and radiation dose data are summarized in Table 2. There were no significant differences with respect to patient age, weight, height, body mass index, prevalence of diabetes and hypertension, menstruation state, maximal tumor diameter, position, or concomitant signs ($P > 0.05$) between the MEI $(+)_{300}$ group and CTA_{370} group. According to our protocol, the mean cumulative CT dose index volume and the mean dose length product were not significantly different between the MEI $(+)_{300}$ group (5.35 ± 1.10 mGy, 160.6 ± 71.94 mGy cm, respectively) and the CTA_{370} group (5.02 ± 1.87 mGy, 156.3 ± 74.7 mGy cm) ($P > 0.05$). The MEI $(+)_{300}$ group intake (195 mg/kg) has less iodine content than CTA_{370} group.

Objective Image Analysis

The mean intraclass correlation coefficient, calculated to quantify interobserver variability, was 0.937 (0.831–0.978). As the x-ray energy decreased, the mean attenuations (Fig. 1A), SDs (Fig. 1B), SNRs (Fig. 1C), and CNRs (Fig. 1D) of the 5 arterials supply of NAC gradually increased. The highest CNR and SNR were observed at 40 keV among the MEIs $(+)_{300}$ and standard linear-blended polyenergetic image. Thereafter, we used the 40 keV MEI $(+)_{300}$ for comparison. Compared with the CTA_{370} group, the 40 keV MEI $(+)_{300}$ yielded significantly higher attenuation in the 5 arterials supply of that NAC (428.72 ± 125.80 vs 225.00 ± 50.15, $P < 0.001$) but also resulted in higher noise (53.37 ± 23.54 vs 18.79 ± 11.53 $P < 0.001$). Both the SNR and CNR were higher in the 40 keV MEI $(+)_{300}$ (SNR, 64.78 ± 28.50 vs 26.29 ± 8.68; CNR, 55.92 ± 27.15 vs 18.79 ± 7.46; both $P < 0.001$) than in the CTA_{370} group (Table 3).

Subjective Image Analysis

A total of 58 and 50 source vessels that provided the dominant blood perfusion to NAC tissues were identified in the 40 keV MEI $(+)_{300}$ group and CTA_{370} group, respectively, and the average number of dominant arteries per breast was 2.32 ± 0.75 and 2.17 ± 0.72 ($P = 0.494$), respectively (Table 4). Among the source vessels in the 2 groups, 24 (41.4%) and 22 (44.0%) were identified as the internal thoracic artery (Fig. 2), 18 (31.0%) and 16 (20.0%) as the lateral thoracic artery (Fig. 3), 11 (18.9%) and 8 (16.0%) as the thoracoacromial artery, and 5 (8.6%) and 4 (8.0%) as the intercostal artery. No vessels from the axillary artery were identified as contributing to NAC perfusion in this study ($P = 0.981$).

The mean ± SD image quality scores of the 40 keV MEI $(+)_{300}$ group and CTA_{370} group were 4.64 ± 0.49 and 4.78 ± 0.42, respectively. This difference was not significant ($P = 0.287$), indicating that the quality of the images from the 40 keV MEI $(+)_{300}$ group was comparable with that of the images from the CTA_{370} group (Table 4). The mean visualization score of the arterials supply

TABLE 4. Subjective Analysis of Images Between the 40 keV MEI $(+)_{300}$ Group and CTA_{370} Group

Parameters	40 keV MEI $(+)_{300}$ Group	CTA_{370} Group	*P*
No. dominant arteries	58	50	
Axillary artery	0	0	0.981
Thoracoacromial artery	11	8	
Lateral thoracic artery	18	16	
Internal thoracic artery	24	22	
Intercostal artery	5	4	
Average dominant arteries per breast	2.32 ± 0.75	2.17 ± 0.72	0.494
Image quality	4.64 ± 0.49	4.78 ± 0.42	0.287
Visualization	1.76 ± 0.44	1.82 ± 0.39	0.583

Data are presented as mean ± SD.

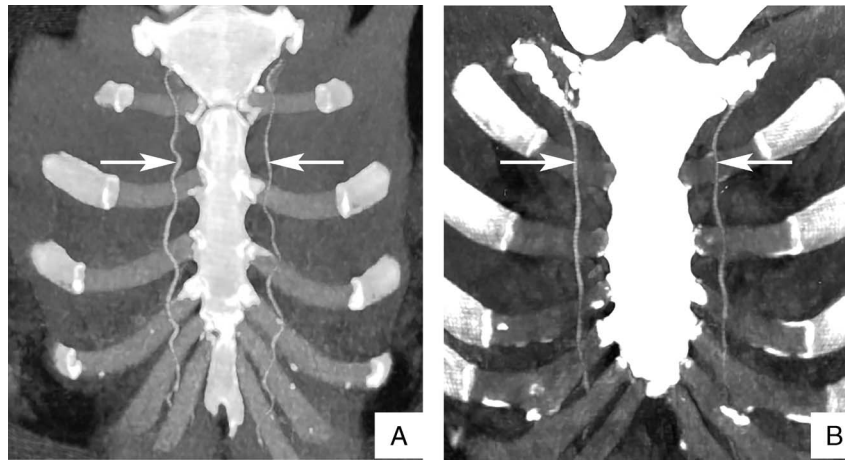

FIGURE 2. Reformatted maximum-intensity projection images of a 52-year-old woman and a 47-year-old woman with right breast cancer obtained by CTA_{370} (A) and 40 keV MEI $(+)_{300}$ (B), respectively. The quality of the CTA_{370} image is slightly better than that of the 40 keV MEI $(+)_{300}$. The visualization of the internal thoracic artery was comparable between CTA_{370} and 40 keV MEI $(+)_{300}$. The arrow points to the internal thoracic artery.

to NAC in the CTA_{370} group was slightly higher than that in the 40 keV MEI $(+)_{300}$ group (1.82 ± 0.39 and 1.76 ± 0.44, respectively), but this difference was not statistically significant ($P = 0.583$) (Table 4).

DISCUSSION

Our study demonstrated that 40 keV MEI $(+)_{300}$ acquired from DECT can improve image quality of the arterial supply to the NAC with low-concentration and low-flow-rate contrast media in breast cancer. We observed greater intravascular attenuation, SNR, and CNR with 40 keV MEI $(+)_{300}$ acquired from DECT; at the same time, the image noise was also increased, which resulted in a comparable subjective image quality score and visualization of the 5 arterials supply to the NAC compared with those of conventional CTA_{370}.

Dual-energy CT provides a wide range of postprocessing functions for evaluating DECT angiography data sets.[21] Previous studies have shown that DECT angiography has potentially greater diagnostic accuracy in the evaluation of vascular stenosis than conventional CTA.[22,23] In addition, DECT angiography can be beneficial for virtual bone removal to improve vascular visualization[24] and in reconstructing virtual, unenhanced images, which has been shown to reduce radiation exposure.[25] To minimize patient exposure to ionizing radiation, our DECT protocols operate using an online dose modulation system (CARE Dose4D; Siemens Healthineers) that adapts the tube current to the patient's anatomy.[26] Low–kiloelectron volt MEIs (+) derived from DECT angiography data allow an improved balance between iodine attenuation and image noise and a reduced amount of contrast media a priori[27] by assessing the CNR and SNR, and have shown superior image quality in DECT angiography. Several studies have shown that the iodine load for abdominal CTA can be reduced by up to 50% with the use of MEI at 40 to 60 keV (reduction in iodine dose, −49%,[28] −27%,[29] and −28%[30]) compared with single-energy CT while providing an equivalent or improved CNR as well as superior subjective image quality. In accordance with those studies, the optimal kiloelectron volt was 40 in the present study, closer to the K-edge of iodine (33 keV); therefore, the attenuation of the arteries could be increased even at a lower concentration of contrast media. We chose a low flow rate to reduce the risk of iodine extravasation. In this study, no extravasation was observed in all patients.

In vast majority of studies, the dominant blood supply to the NAC seems to be attributed to the internal thoracic artery and/or the lateral thoracic artery. One study[31] showed that the internal

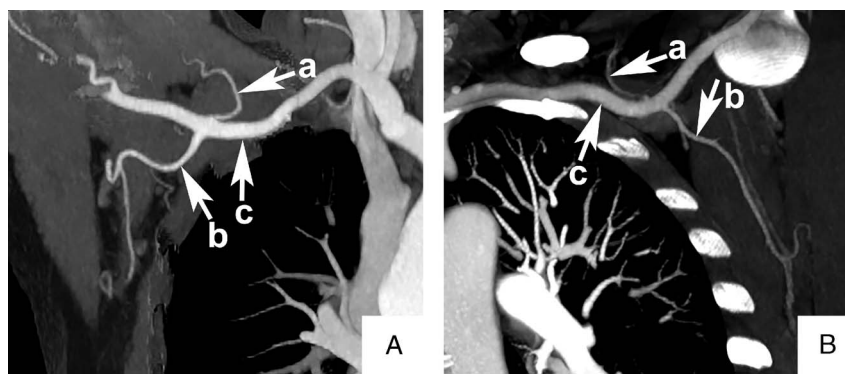

FIGURE 3. Reformatted maximum-intensity projection images of a 50-year-old woman with right breast cancer and a 54-year-old woman with left breast cancer obtained by CTA_{370} (A) and 40 keV MEI $(+)_{300}$ (B), respectively. Visualization of the thoracoacromial artery (arrow a), lateral thoracic artery (arrow b), and axillary artery (arrow c) was excellent in both groups.

thoracic artery is the most important breast blood supply source, and even within the same individual, blood supply types are diverse and asymmetrical. Later, another study,[4] based on the results from a microdissection technique, demonstrated that the lateral thoracic artery is the most dominant blood supply source of the NAC, followed by the internal thoracic artery. In our study, the internal thoracic artery and the lateral thoracic artery accounted for 72.4% (42/58) and 76.0% (38/50) of the dominant blood supply to the NAC in the 2 groups, respectively, consistent with previous studies. In the 2 groups, we observed no difference in the number of average dominant arteries per breast for different contrast media protocols.

Recently, a noise-optimized MEI (+) reconstruction algorithm was developed to perform spatial frequency-based recombination, which results in the highest possible image contrast by reducing the image noise at lower energy levels.[32] In our study, image noise was increased in the 40 keV MEI $(+)_{300}$ group compared with that of the CTA_{370} group, which is consistent with previous results.[16] However, subjectively, there was no statistically significant or clinical difference in the perceived image noise between the 2 groups, especially in the evaluation of the arteries. This may be due to that it is difficult to visually separate additional image spots when arterial attenuation is significantly improved.[33] These data show that image noise should not be an obstacle to the use of low kiloelectron volt. Computed tomography angiography can be performed effectively with a low concentration and flow rate of contrast media without a clinically significant noise penalty, which is of great benefit to patients with breast cancer with impaired renal function or suboptimal venous access. Studies involving patients with specific breast cancers will help provide further insight into the relative value of the 2 DECT angiography techniques with different concentrations of contrast media.

This study has several important limitations. First, we limited this investigation to the analysis of intravascular attenuation, SD measurements, and subjective scoring, comparing a 40 keV MEI $(+)_{300}$ group and a CTA_{370} group, where the imaging parameters were selected to match the radiation dose. We did not attempt to assess diagnostic accuracy or vascular findings during the clinical operation. Second, we compared 40 keV MEI $(+)_{300}$ with CTA_{370} images, which were derived from DECT rather than single-energy CT; the conclusions obtained here were identical to those obtained for single-energy CT-derived images. Third, our study included a relatively small patient cohort, and we did not evaluate the traditional monoenergetic reconstruction algorithm, which has shown poor results at low kiloelectron volt levels.

In summary, our study demonstrated that 40 keV MEI $(+)_{300}$ acquired from DECT can improve image quality of the arterial supply to the NAC with low-concentration and low-flow-rate contrast media in breast cancer. Duel-energy CT with low-concentration and low-flow-rate contrast media can be used not only to routinely screen lung metastases of breast cancer but also to provide valuable information about the blood supply to the NAC to aid in the design of custom treatments through MEIs (+). This method can reduce the iodine dose for patients with breast cancer.

ACKNOWLEDGMENTS

The authors thank all volunteers who participated in the study and the staff of the Department of Radiology, Chongqing University Cancer Hospital, Chongqing Cancer Institute, and Chongqing Cancer Hospital in Chongqing, China, for their selfless and valuable assistance.

REFERENCES

1. Bray F, Ferlay J, Soerjomataram I, et al. Global cancer statistics 2018: GLOBOCAN estimates of incidence and mortality worldwide for 36 cancers in 185 countries. *CA Cancer J Clin*. 2018;68:394–424. doi: 10.3322/caac.21492.
2. Bailey CR, Ogbuagu O, Baltodano PA, et al. Quality-of-life outcomes improve with nipple-sparing mastectomy and breast reconstruction. *Plast Reconstr Surg*. 2017;140:219–226. doi:10.1097/prs.0000000000003505.
3. Seitz IA, Nixon AT, Friedewald SM, et al. "NACsomes": a new classification system of the blood supply to the nipple areola complex (NAC) based on diagnostic breast MRI exams. *J Plast Reconstr Aesthet Surg*. 2015;68:792–799. doi:10.1016/j.bjps.2015.02.027.
4. O'Dey DM, Prescher A, Pallua N. Vascular reliability of nipple-areola complex-bearing pedicles: an anatomical microdissection study. *Plast Reconstr Surg*. 2007;119:1167–1177. doi:10.1097/01.prs.0000254360.98241.dc.
5. Zheng H, Su Y, Zheng M, et al. Computed tomographic angiography-based characterization of source blood vessels for nipple-areola complex perfusion in hypertrophic breasts. *Aesthetic Plast Surg*. 2017;41:524–530. doi:10.1007/s00266-017-0791-5.
6. Strauch B, Elkowitz M, Baum T, et al. Superolateral pedicle for breast surgery: an operation for all reasons. *Plast Reconstr Surg*. 2005;115:1269–1277; discussion 1278-1269. doi:10.1097/01.prs.0000156981.63447.6d.
7. Berthe JV, Massaut J, Greuse M, et al. The vertical mammaplasty: a reappraisal of the technique and its complications. *Plast Reconstr Surg*. 2003;111:2192–2199; discussion 2200-2192. doi:10.1097/01.prs.0000062621.83706.88.
8. Keys KA, Louie O, Said HK, et al. Clinical utility of CT angiography in DIEP breast reconstruction. *J Plast Reconstr Aesthet Surg*. 2013;66:e61–e65. doi:10.1016/j.bjps.2012.09.025.
9. Pratt GF, Rozen WM, Chubb D, et al. Preoperative imaging for perforator flaps in reconstructive surgery: a systematic review of the evidence for current techniques. *Ann Plast Surg*. 2012;69:3–9. doi:10.1097/SPA.0b013e318222b7b7.
10. Rozen WM, Anavekar NS, Ashton MW, et al. Does the preoperative imaging of perforators with CT angiography improve operative outcomes in breast reconstruction? *Microsurgery*. 2008;28:516–523. doi:10.1002/micr.20526.
11. Wade RG, Watford J, Wormald JCR, et al. Perforator mapping reduces the operative time of DIEP flap breast reconstruction: a systematic review and meta-analysis of preoperative ultrasound, computed tomography and magnetic resonance angiography. *J Plast Reconstr Aesthet Surg*. 2018;71:468–477. doi:10.1016/j.bjps.2017.12.012.
12. Bae KT. Optimization of contrast enhancement in thoracic MDCT. *Radiol Clin North Am*. 2010;48:9–29. doi:10.1016/j.rcl.2009.08.012.
13. Delesalle MA, Pontana F, Duhamel A, et al. Spectral optimization of chest CT angiography with reduced iodine load: experience in 80 patients evaluated with dual-source, dual-energy CT. *Radiology*. 2013;267:256–266. doi:10.1148/radiol.12120195.
14. Mitsumori LM, Wang E, May JM, et al. Triphasic contrast bolus for whole-chest ECG-gated 64-MDCT of patients with nonspecific chest pain: evaluation of arterial enhancement and streak artifact. *AJR Am J Roentgenol*. 2010;194:W263–W271. doi:10.2214/ajr.09.2788.
15. Beckett KR, Moriarity AK, Langer JM. Safe use of contrast media: what the radiologist needs to know. *Radiographics*. 2015;35:1738–1750. doi:10.1148/rg.2015150033.
16. He J, Wang Q, Ma X, et al. Dual-energy CT angiography of abdomen with routine concentration contrast agent in comparison with conventional single-energy CT with high concentration contrast agent. *Eur J Radiol*. 2015;84:221–227. doi:10.1016/j.ejrad.2014.11.025.
17. Ohtsu Y, Gibbons JA, Suzuki K, et al. Absorption, distribution, metabolism, and excretion of the androgen receptor inhibitor enzalutamide in rats and dogs. *Eur J Drug Metab Pharmacokinet*. 2017;42:611–626. doi:10.1007/s13318-016-0374-x.

18. Ueguchi T, Ogihara R, Yamada S. Accuracy of dual-energy virtual monochromatic CT numbers: comparison between the single-source projection-based and dual-source image-based methods. *Acad Radiol*. 2018;25:1632–1639. doi:10.1016/j.acra.2018.02.022.

19. Patino M, Parakh A, Lo GC, et al. Virtual monochromatic dual-energy aortoiliac CT angiography with reduced iodine dose: a prospective randomized study. *AJR Am J Roentgenol*. 2019;212:467–474. doi:10.2214/ajr.18.19935.

20. Shuman WP, O'Malley RB, Busey JM, et al. Prospective comparison of dual-energy CT aortography using 70% reduced iodine dose versus single-energy CT aortography using standard iodine dose in the same patient. *Abdom Radiol (NY)*. 2017;42:759–765. doi:10.1007/s00261-016-1041-z.

21. Vlahos I, Chung R, Nair A, et al. Dual-energy CT: vascular applications. *AJR Am J Roentgenol*. 2012;199:S87–S97. doi:10.2214/ajr.12.9114.

22. Brockmann C, Jochum S, Sadick M, et al. Dual-energy CT angiography in peripheral arterial occlusive disease. *Cardiovasc Intervent Radiol*. 2009;32:630–637. doi:10.1007/s00270-008-9491-5.

23. Huang SY, Nelson RC, Miller MJ, et al. Assessment of vascular contrast and depiction of stenoses in abdominopelvic and lower extremity vasculature: comparison of dual-energy MDCT with digital subtraction angiography. *Acad Radiol*. 2012;19:1149–1157. doi:10.1016/j.acra.2012.04.014.

24. Sommer WH, Johnson TR, Becker CR, et al. The value of dual-energy bone removal in maximum intensity projections of lower extremity computed tomography angiography. *Invest Radiol*. 2009;44:285–292. doi:10.1097/RLI.0b013e31819b70ba.

25. Buffa V, Solazzo A, D'Auria V, et al. Dual-source dual-energy CT: dose reduction after endovascular abdominal aortic aneurysm repair. *Radiol Med*. 2014;119:934–941. doi:10.1007/s11547-014-0420-1.

26. Graser A, Wintersperger BJ, Suess C, et al. Dose reduction and image quality in MDCT colonography using tube current modulation. *AJR Am J Roentgenol*. 2006;187:695–701. doi:10.2214/ajr.05.0662.

27. Rajiah P, Abbara S, Halliburton SS. Spectral detector CT for cardiovascular applications. *Diagn Interv Radiol*. 2017;23:187–193. doi:10.5152/dir.2016.16255.

28. Shuman WP, Chan KT, Busey JM, et al. Dual-energy CT aortography with 50% reduced iodine dose versus single-energy CT aortography with standard iodine dose. *Acad Radiol*. 2016;23:611–618. doi:10.1016/j.acra.2015.12.019.

29. Agrawal MD, Oliveira GR, Kalva SP, et al. Prospective comparison of reduced-iodine-dose virtual monochromatic imaging dataset from dual-energy CT angiography with standard-iodine-dose single-energy CT angiography for abdominal aortic aneurysm. *AJR Am J Roentgenol*. 2016;207:W125–W132. doi:10.2214/ajr.15.15814.

30. Xin L, Yang X, Huang N, et al. The initial experience of the upper abdominal CT angiography using low-concentration contrast medium on dual energy spectral CT. *Abdom Imaging*. 2015;40:2894–2899. doi:10.1007/s00261-015-0462-4.

31. van Deventer PV. The blood supply to the nipple-areola complex of the human mammary gland. *Aesthetic Plast Surg*. 2004;28:393–398. doi:10.1007/s00266-003-7113-9.

32. Beer L, Toepker M, Ba-Ssalamah A, et al. Objective and subjective comparison of virtual monoenergetic vs. polychromatic images in patients with pancreatic ductal adenocarcinoma. *Eur Radiol*. 2019;29:3617–3625. doi:10.1007/s00330-019-06116-9.

33. Godoy MC, Naidich DP, Marchiori E, et al. Single-acquisition dual-energy multidetector computed tomography: analysis of vascular enhancement and postprocessing techniques for evaluating the thoracic aorta. *J Comput Assist Tomogr*. 2010;34:670–677. doi:10.1097/RCT.0b013e3181e10627.